Fuel Efficient Rudder and Propeller Control Allocation for Marine Craft: Experiments with a Model Ship

Karl-Petter Lindegaard and Thor I. Fossen

Submitted to IEEE Transactions on Control Systems Technology
Paper No. 2002-047

Submitted	February 20, 2002
First revision	September 22, 2002
Second revision	January 27, 2003

The authors are with the Department of Engineering Cybernetics, Norwegian University of Science and Technology, N-7491 Trondheim, Norway. E-mail: kpl@itk.ntnu.no, tif@itk.ntnu.no

Supported by the Norwegian Research Council through the strategic university program on marine cybernetics

Abstract

We derived a control allocation algorithm for low speed marine craft using propellers and rudders. Active use of rudders has advantages in a low-speed operation by decreasing the need for propeller power and fuel. However, at low speed a rudder is effective only for positive thrust. This complicates the thrust allocation problem which can no longer be solved by convex quadratic programming. In fact, the existence of local minima introduces discontinuities in the commanded thruster signals even if the desired control force is continuous. Discontinuous signals cause excessive wear on the thruster system and must be avoided. This paper suggests an analytic 2-norm optimal method that can ensure continuity of the solutions. Due to it being analytic its limitation is, however, that it is capable of handling only configurations where one single thrust device is subject to sector constraints at a time. Experiments with a model ship illustrate the potential for fuel saving. For this particular vessel the energy consumption was cut in half. An output feedback tracking control law with integral action was simultanously derived and analyzed. Semi-global ship controllers like this one rely on the yaw rate being bounded, and an admittedly conservative method for determining this upper bound was proposed.

Keywords

Marine vehicle control, fuel optimal control, nonlinear systems, output feedback, asymptotic stability.

I. Introduction

Automatic control of ships has been studied for almost a century. In 1911 *Elmer Sperry* constructed the first automatic ship steering mechanism called *"Metal Mike"*. Today, the range of marine vessels is expanded to a huge diversity of vehicles such as remotely operated vehicles (ROVs) and semi-submersible rigs. Automatic control systems for heading and depth control, way-point tracking control, fin and rudder-roll damping, dynamic positioning (DP), position mooring etc. are commercial products [1]. A commercial control system is usually designed as three interconnected subsystems for *Guidance*, *Navigation* and *Control* (GNC). The control system block contains a *feedback control law* and a *control allocation* (CA) algorithm needed for optimal distribution of controller commands to the different actuators.

The main contribution of this paper is a thrust and rudder (control) allocation algorithm for marine vessels. This is a challenging problem since a ship at zero speed with a main propeller and a single rudder produces lift (sideforce) for positive propeller revolutions only. Rudder forces are approximately zero when the propeller is reversed. The rudder force is also limited to a small sector due to rudder angle saturation.

Optimal thrust allocation in station-keeping has been addressed previously [2], [3], [4], [5], [6]. However, we believe that simultaneous thrust and rudder allocation for ships at zero speed has not received so much attention. Since operating a rudder servo is relatively inexpensive compared to operating a propeller, this gives a large fuel saving potential. This solution is well known in practice since experienced Captains use a non-zero rudder angle (for positive thrust) in station-keeping and docking to produce additional forces in the transverse direction. In this paper a constrained rudder/propeller control allocation algorithm is derived in conjuncture with a Lyapunov stable output feedback controller for low speed tracking.

For ships with more control inputs than controllable degrees of freedom (DOF), it is possible to find an "optimal" distribution of control forces $F \in \mathbb{R}^p$ provided that the demand is attainable. Here p is the number of actuators/propulsive devices which can be operated individually. The commanded generalized

force (forces and moments), τ_c, is generated by a higher-level controller e.g. a dynamic positioning system. In this context a higher-level controller may be any arbitrary automatic control law (see Figure 1), or it could be a joystick operator manually commanding surge and sway forces as well as a yaw moment (Figure 2). Regardless of the source of commanded forces, the CA algorithm is responsible for calculating an "optimal" solution of actuator set-points that at all times satisfy the presumed attainable commanded generalized force signal.

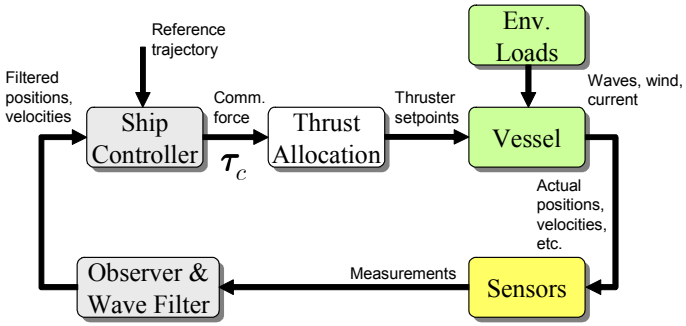

Fig. 1. Overview of an automatic ship control system with a high level controller.

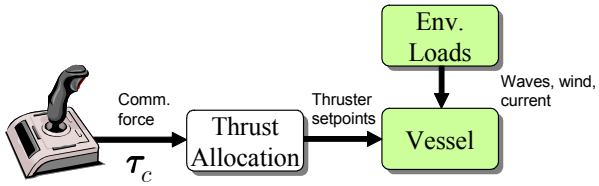

Fig. 2. Overview of a manual joystick control system.

In general CA is a dynamic nonlinear optimization problem since there are sector limitations for operation of the rudders and the rotatable thrusters (azimuth thrusters). This problem can be solved using nonlinear optimization techniques [7] e.g. quadratic programming (QP), see Lindfors [3]. An alternative method using the singular value decomposition and a filtering scheme to control the azimuth directions has been proposed by Sørdalen [4] who also presented results from sea trials [5]. A similar technique using the damped least squares algorithm has been reported in [6].

The allocation part of ship control has received very little attention compared to emphasis put down in advanced controller and filter design [4]. This lack of attention is unfortunate, because the performance of an automatic control system will suffer if the CA module is poorly designed. Moreover, the design of the allocation module is the decisive element determining the costs, in terms of energy consumption, of obtaining the desired level of performance. An efficient CA algorithm requires less power than a less efficient one. Consequently, an efficient scheme will reduce the fuel consumption and simultaneously decrease gas emissions.

While the mentioned CA schemes for ships perform an unconstrained optimization, the aerospace community has addressed constrained CA methods for quite some time. The two most frequently reported strategies are Durham's tailor-made generalized inverses [8], [9], [10], [11], [12], [13] and actuator daisy chaining [14], [15], [16]. The set of admissible controls is usually an n-dimensional rectangle, as in the tailor-made inverses, and the controls can be selected independently of each other. These methods do not apply to ships with rotatable thrusters or rudders. Neither is the set of admissible controls necessarily convex, nor will the controls be independent. Another difference between an aircraft and a ship is how a universal cost criterion should be defined. For a ship at low speed it is an obvious goal to minimize the total thrust force (and thereby fuel consumption) while for a cruising airplane the cost of using the passive control surfaces in terms of energy is of minor importance, although minimizing the drag has been considered.

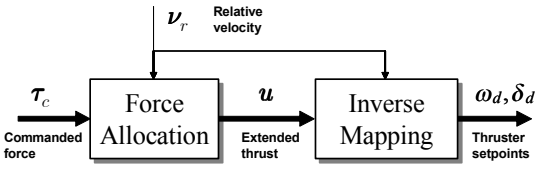

Fig. 3. The thrust allocation problem seen as a two-step process.

The control allocation problem arises in cases where there are more actuators than DOFs, or more precisely when the decision variables u outnumber the constraints. An algorithm can be divided into two steps as described in Figure 3. In the first step, called force allocation, the commanded generalized force τ_c is distributed out to each one of the p available actuators. It is the decision made at this stage that is going to determine how "good" the algorithm is. The second step deals with finding which actuator set-points will generate the desired forces F. This step is called "inverse mapping" because it must solve the inverse of the actuator models. The vessel's velocity relative to the fluid ν_r is considered an auxiliary signal that must be accounted for since rudder forces depend greatly on surge velocity. Evidently, the thrust models used in the second step influence the domain of u. For low speed applications, as considered in this paper, the ship's relative velocity ν_r may be neglected.

The thrust allocation problem is an optimization problem with several requirements to consider. For instance, the algorithm must take into account the capacity of each thrust device and it must avoid "singular solutions" [4], [17] that produce unacceptably large thrust magnitudes. Furthermore, finding a suitable solution must take a minimum of time and computational effort because the implementation runs on a real-time platform often with limited resources. More sophisticated algorithms should include support for thrusters with a preferred thrusting direction (many thrust devices are more effective when producing positive thrust than negative) and also take into account the dynamic constraints of the propulsion system, e.g. a rotatable thruster cannot rotate arbitrarily fast (rate saturation). Those issues will, however, not

be addressed here.

A topic related to saturation handling is to determine attainable thrust set [8], [9], [10], that is all combinations of τ_c that the thruster system can provide. Limitations will be imposed by the maximum capacity of each device (box constraints), but also by the amount of available power on the power buses on which the thrusters are connected. If rate limitations are to be handled, the current states influence the attainable thrust too. By analyzing the attainable set before sending the demand τ_c to the force allocation module (Figure 3) or at least taking it into account in the allocation itself, we are given the opportunity to analyze and modify the demand in light of the limitations. The desired τ_c should be checked to see whether or not it is attainable, and if it is not, explicit action must be taken because overall control of the resulting thrust will be lost if the actuators are limited individually after the inverse mapping. In such cases one approach could be to give preference to some of the controllable DOFs in the τ_c-vector and to modify the other ones such that τ_c eventually becomes attainable. In aerospace applications the set of attainable thrust is convex [9], [10] simplifying such priority considerations significantly. This is, however, not the case for ships with sector restricted rotatable thrusters or propeller-rudder pairs. Because of this non-convexity, it will be beyond the scope of this paper to pursue this topic further. Instead we assume that τ_c is always attainable.

II. Problem Statement

A. Notation and Definitions

Consider a vessel with p actuators. By an actuator we mean rotatable or fixed propellers, waterjets and other devices capable of producing a propulsive force. A main propeller equipped with a rudder is considered a rotatable device. Passive devices such as standalone rudders and flaps are to be considered to be actuators at non-zero velocities, while at velocities near zero they should not.

Assume there are p_r rotatable and p_f fixed force devices such that $p = p_r + p_f$. Notice that a rotatable actuator has two controls, one for the direction and one for force amplitude. For the rotatable and fixed actuators this yields $n_r = 2p_r$ and $n_f = p_f$ number of decision variables respectively. In sum there are $n = n_r + n_f$ decision variables. Let q denote the number of DOFs under consideration, and if $2p_r + p_f > q$ the vessel is said to be *overactuated*. From now on we shall consider *surge*, *sway* and *yaw* only, thus $q = 3$.

Each thruster k is located at

$$r_k = \begin{bmatrix} l_{k,x} & l_{k,y} \end{bmatrix}^T \tag{1}$$

with respect to the origin of the vessel-fixed coordinate system and can produce a force F_k in a direction α_k. The x-axis points forward and the y-axis to the right (starboard).

The difference between the rotatable thrusters numbered $1 \leq k \leq p_r$ and fixed thrusters $p_r + 1 \leq k \leq p$ is that the direction α_k can be manipulated.

Let $F_k^{\max} > 0$ be the maximum thrust force such that the *normalized thrust* ρ_k defined as

$$\rho_k = \frac{1}{F_k^{\max}} F_k \tag{2}$$

satisfies $|\rho_k| \leq 1$ for all k. Define $\mathcal{I}$ as a subset of $\mathbb{R}$

$$\mathcal{I} = \{x \in \mathbb{R} \,|-1 \leq x \leq 1\} \tag{3}$$

Then $\rho_k \in \mathcal{I}$ and $\rho \in \mathcal{I}^p$.

The sum of *generalized forces* on the vessel $\tau \in \mathbb{R}^3$ is

$$\tau = \underbrace{\bar{A}(\alpha)}_{\substack{\text{configuration} \\ \text{matrix}}} \underbrace{\bar{F}\rho}_{\text{thrust}} \tag{4}$$

where

$$\bar{A}(\alpha) = \begin{bmatrix} \cos\alpha_1 & \cdots & \cos\alpha_p \\ \sin\alpha_1 & & \sin\alpha_p \\ -l_{1,y}\cos\alpha_1 + l_{1,x}\sin\alpha_1 & \cdots & -l_{p,y}\cos\alpha_p + l_{p,x}\sin\alpha_p \end{bmatrix} \tag{5}$$

$$\bar{F} = \text{diag}\{F_1^{\max}, ..., F_p^{\max}\} \tag{6}$$

The vessel is said to be in a *singular configuration* if $\bar{A}(\alpha)$ looses rank due to a poor selection of α.

Let $u \in \mathcal{I}^n$ denote the control vector where the normalized thrust ρ_k for each thruster has been decomposed in the horizontal plane according to:

$$u_{k,x} = \rho_k \cos\alpha_k \quad , \quad u_{k,y} = \rho_k \sin\alpha_k \tag{7}$$

The decomposition u is called *extended thrust*. Let Π_k be a projection that extracts the extended thrust vector u_k of thruster k from u according to

$$u_k = \Pi_k u \tag{8}$$

For rotatable thrusters $u_k \in \mathcal{I}^2$, $1 \leq k \leq p_r$ and for fixed thrusters $p_r + 1 \leq k \leq p$ we have $u_k = \rho_k \in \mathcal{I}$.

Most likely an extended thrust u_k is confined to a domain of $\mathcal{I}^2$ (or $\mathcal{I}$), e.g. an azimuth thruster could be restricted to thrust only inside a predefined sector. Let each extended thrust u_k be confined to the domain $\mathcal{D}_k$, that is for $k \in [1..p_r]$ we have $\mathcal{D}_k \subset \mathcal{I}^2$ and for $k > p_r$, $\mathcal{D}_k \subset \mathcal{I}$.

Using the concept of extended thrust, the generalized thrust vector τ becomes

$$\tau = BF_u u \tag{9}$$

where $B \in \mathbb{R}^{3\times n}$ consists of $B_r \in \mathbb{R}^{3\times n_r}$ and $B_f \in \mathbb{R}^{3\times n_f}$

$$B = \begin{bmatrix} B_r & B_f \end{bmatrix} \tag{10}$$

$$B_r = \begin{bmatrix} 1 & 0 & \cdots & 1 & 0 \\ 0 & 1 & \cdots & 0 & 1 \\ -l_{1,y} & l_{1,x} & \cdots & -l_{n_r,y} & l_{n_r,x} \end{bmatrix} \tag{11}$$

$$B_f = \begin{bmatrix} \cos\alpha_{p_r+1} & \cdots & \cos\alpha_p \\ \sin\alpha_{p_r+1} & \cdots & \sin\alpha_p \\ -l_{p_r+1,y}\cos\alpha_{p_r+1} + l_{p_r+1,x}\sin\alpha_{p_r+1} & \cdots & -l_{p,y}\cos\alpha_p + l_{p,x}\sin\alpha_p \end{bmatrix} \tag{12}$$

Notice that B is a constant matrix of rank q (here $q = 3$) whenever the craft is overactuated. The matrix $F_u \in \mathbb{R}^{n\times n}$ is a diagonal matrix with corresponding values of $F_k^{\max}$ along the diagonal. Define:

$$A = BF_u \tag{13}$$

A control vector u (extended thrust) is called *feasible* if the linear constraint

$$f = Au - \tau_c = 0 \tag{14}$$

and each and every $u_k = \Pi_k u$ lies in its domain $\mathcal{D}_k$.

Let the columns in the matrix N be an orthonormal basis of the null-space $\mathcal{N}(A)$. Then, $AN = 0$. The null-space $\mathcal{N}(A)$ and row-space of A, denoted $\mathcal{R}(A^T)$, are orthogonal subspaces of $\mathbb{R}^n$.

The *generalized inverse* of a matrix A, using a symmetric and positive definite weight matrix $W = W^T > 0$, is defined as:

$$A^\dagger = W^{-1}A^T\left(AW^{-1}A^T\right)^{-1} \tag{15}$$

such that the unconstrained solution:

$$u_* = A^\dagger \tau_c \tag{16}$$

is the optimal solution, in a weighed 2-norm sense, that is

$$u_*^T W u_* \leq u^T W u \quad \forall \quad \{u \in \mathbb{R}^n \,|Au - \tau_c = 0\} \tag{17}$$

Moreover, $u_* \in \mathcal{R}(W^{-1}A^T)$.

If $W = I$, we get the *pseudo-inverse*

$$A^+ = A^T\left(AA^T\right)^{-1} \tag{18}$$

such that $u_* \in \mathcal{R}(A^T)$. Without loss of generality, we use A^+ instead of $A^\dagger$ in calculating the unconstrained solution.

B. Problem Introduction

The main objective of this paper was finding a feasible control vector u (extended thrust) that is optimal with respect to some cost function quadratic in u.

Quadratic cost functions are attractive candidates because when the domains $\mathcal{D}_k$ are described by linear inequalities the problem is a general quadratic program (QP). Quadratic programs can be solved in a finite number of iterations and are consequently quite predictable which again makes them well suited for real-time implementation. Unfortunately, a propeller-rudder device requires a non-convex domain $\mathcal{D}_k$ because these propulsive devices are unable to produce lateral forces without simultaneously generating significant longitudinal forces.

It is reasonable to assume that the rudder is capable of producing lift for positive thrust force (forward). For negative longitudinal force the rudder can be regarded as inactive, thus the attainable set shrinks to a thin line. Typically the physically attainable thrust region resembles a twisted circular sector, represented by the grid in Figure 4. Notice that the negative x-axis is also a part of the attainable set. For convenience, the grid is approximated by an inscribed circular sector so that the feasible set $\mathcal{D}_k$ is given by this sector element and the negative x-axis.

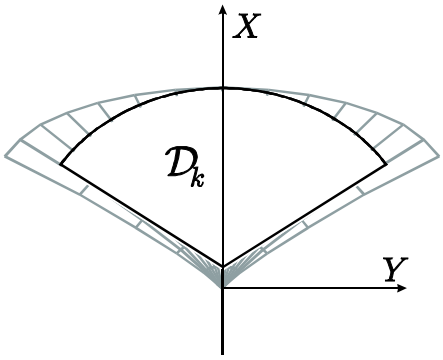

Fig. 4. The physically attainable thrust region (grid) for a propeller-rudder pair. An inscribed circular sector and the negative x-axis together serve as the feasible region $\mathcal{D}_k$.

Even though a sequential QP (SQP) or a sequential linearly constrained (SLC) method does find a solution, careless utilization of any numerical method can lead to unintended results:

1. An SQP method solves a sequence of QP problems and is therefore more computationally demanding than a single QP. Moreover, if the iteration sequence is interrupted or preempted due to CPU time limitations, the current solution may not be optimal.
2. The non-convex inequality constraints for the propeller-rudder couple introduce a discontinuity in the mapping from $\tau_c \rightarrow u$ if the optimal solution is to be used at all times.

This second disadvantage must be handled explicitly. Infinitesimal changes in τ_c should never lead to discontinuous extended thrust u.

The situation is illustrated in Figure 5. The optimal unconstrained solution for thruster k, that is $u_{*,k}$, is marked with a cross and the dotted cost curves illustrate the cost involved getting the solution into the feasible domain $\mathcal{D}_k$. The two circles mark feasible solutions with identical cost. Since the unconstrained solution $u_{*,k}$ lies slightly above the *equicost line* (dashed) the uppermost solution is selected. Once $u_{*,k}$

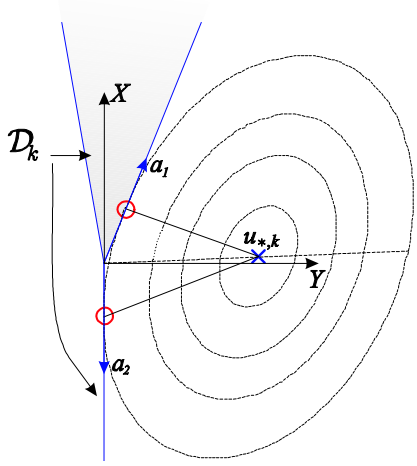

Fig. 5. Illustration of a discontinuous mapping from τ_c to generalized force vector u.

crosses the equicost, the lower solution becomes optimal. Hence, the mapping is discontinuous and this will again cause undesired propeller and rudder angle chattering. It is therefore of paramount importance to avoid introducing this discontinuity.

III. Force Allocation

The proposed algorithm is analytic and requires no iterations whatsoever. This means that some assumptions have to be made:

1. Only one thruster, thruster k, with sector constraints is supported.
2. Thrust force magnitude constraints (box constraints) are not considered.

Due to the feasible region being non-convex, it is not straightforward to uncritically apply re-allocation if one or more of the thrust devices should saturate. Re-allocating by looping through all possible configurations [18] can also be time-consuming. Still, our method is 2-norm optimal, it does avoid rudder-chattering and it does produce continuous solutions. The two latter properties have, as far as we know, not been considered elsewhere, but any CA algorithm for ships should support them.

Assumption 1 is the key to analytically handle sector constraints and to ensure continuity. The disadvantage is that for configurations where several thrusters are subject to sector constraints, some suboptimal modification must be made, for instance by handling one thruster at a time and keeping the others at a fixed angle. This particular approach was pursued here since the ship was equipped with two propeller-rudder pairs. As a consequence, one rudder only could be used at any one time.

Thruster saturation is not covered according to Assumption 2. Traditionally, iterative solvers distribute possible overshoot from the saturated thrusters onto the remaining ones provided that the demand τ_c is attainable. Without saturation handling, however, we are not guaranteed to obtain the desired τ_c even when it is attainable. But as long as τ_c is comparatively small with respect to the attainable set, no

thruster should saturate and the box constraints can be disregarded. It should be noted that explicit, non-iterative, off-line pre-computed schemes do handle box-constraints [19], but they do not support non-convex constraints.

The algorithm for finding a feasible extended thrust vector u is solved in two steps in order to maximize computational performance. First, an unconstrained solution is found. If this 2-norm optimal solution lies outside the feasible domain $\mathcal{D}$, we need to determine the minimum accumulated cost translating the solution from u_* to the domain $\mathcal{D}$.

A. Unconstrained

The first step in the allocation of extended thrust u is achieved by simply employing the pseudo-inverse in order to minimize the 2-norm of u.

$$u_* = A^+ \tau_c \tag{19}$$

If $u_* \notin \mathcal{D}$ Figure 5 indicates that simply projecting the u_* onto $\mathcal{D}$ one is not guaranteed to end up with a minimum cost $u \in \mathcal{D}$. We have to consider the actual cost accumulated by traversing the null-space $\mathcal{N}(A)$. This is the topic of the next subsection.

B. Sector Constraints

Assume that thrust device k is restricted in a domain $\mathcal{D}_k \subset \mathbb{R}^2$ as illustrated in Figure 5 and that the pseudo-inverse solution u_* has already been found. Since u_* satisfies the linear equality constraint (14), we may add any linear combination of the columns in N denoted $\delta u = N\sigma$ where σ is a vector of appropriate dimension, and still have a solution satisfying the linear equality constraint.

$$u = u_* + \delta u = u_* + N\sigma \tag{20}$$

The objective is now to find the optimal σ which renders u feasible and minimizes $\|u\|_2 \geq \|u_*\|_2$. We have

$$\begin{aligned} \|u\|_2^2 &= (u_* + N\sigma)^T (u_* + N\sigma) \\ &= \|u_*\|_2^2 + \|\sigma\|_2^2 \end{aligned} \tag{21}$$

where we have used that $u_* \in \mathcal{R}(A^T)$ such that $N^T u_* = 0$ and $N^T N = I$ since N is an orthonormal basis. Consequently, we seek a vector σ with minimum 2-norm.

Consider device number k. We have to find an increment δu_k such that $u_k \in \mathcal{D}_k$

$$u_k = u_{*,k} + \delta u_k, \quad \delta u_k = \Pi_k N \sigma \tag{22}$$

Once again the pseudo-inverse comes in handy because it minimizes the 2-norm. Hence,

$$\sigma = (\Pi_k N)^+ \delta u_k \tag{23}$$

is the solution we are looking for, but we have yet to determine δu_k.

Once u_k enters the feasible region spanned by a_1 and a_2 (Figure 5), it is going to be parallel to one linear boundary curve $a_i \in \mathbb{R}^2$. Consequently, we have reached the minimum when $u_k || a_i$, which can be rephrased as a linear constraint because any a_i is a design parameter. By letting $a = a_i$ and using the inner product we get the constraint

$$f_s = a_\perp^T u_k = a_\perp^T \left(u_{*,k} + \delta u_k \right) = 0 \tag{24}$$

where $a_\perp$ is orthogonal to a, that is $a^T a_\perp = 0$. Later, in Section III-D we focus on determining which boundary vector a to use.

Define the Lagrangian

$$\begin{aligned} L &= \frac{1}{2}\sigma^T\sigma + \lambda f_s \\ &= \frac{1}{2}\left(\delta u_k\right)^T W_k \delta u_k + \lambda\left(a_\perp^T u_{*,k} + a_\perp^T \delta u_k\right) \end{aligned} \tag{25}$$

where it can be shown that

$$W_k = \left(\Pi_k N N^T \Pi_k\right)^{-1} \tag{26}$$

is positive definite as long as $\dim \mathcal{N}(A) \geq 2$. In other words N must have at least two columns. It must be pointed out that only the inverse W_k^{-1} will be utilized and not W_k itself. Since we only have to calculate

$$W_k^{-1} = \Pi_k N N^T \Pi_k \tag{27}$$

we may disregard the dimension of the null-space causing a singular W_k.

If $\dim \mathcal{N}(A) \geq 2$ this reduces to an unconstrained QP problem trivially solved using the generalized inverse. The minimum solution is found by minimizing L

$$\frac{\partial L}{\partial \delta u_k} = W_k \delta u_k + a_\perp \lambda = 0 \tag{28}$$

$$\delta u_k = -W_k^{-1} a_\perp \lambda \tag{29}$$

Since the constrained solution is parallel to a, by using (24)

$$\lambda = \left(a_\perp^T W_k^{-1} a_\perp\right)^{-1} a_\perp^T u_{*,k} \tag{30}$$

the optimal solution is

$$\delta u_k = -W_k^{-1} a_\perp \left(a_\perp^T W_k^{-1} a_\perp\right)^{-1} a_\perp^T u_{*,k} \tag{31}$$

For all thrust devices together, the optimal increment δu is obtained by combining (20), (23) and (31)

$$\delta u = N \left(\Pi_k N\right)^+ \delta u_k \tag{32}$$

and hence for the modified extended thrust, assuming $u \in \mathcal{D}$

$$\begin{aligned} u &= u_* - N\left(\Pi_k N\right)^+ W_k^{-1} a_\perp \left(a_\perp^T W_k^{-1} a_\perp\right)^{-1} a_\perp^T u_{*,k} \\ &= \left(I - NN^T \Pi_k^T a_\perp \left(a_\perp^T W_k^{-1} a_\perp\right)^{-1} a_\perp^T \Pi_k\right) u_* \end{aligned} \tag{33}$$

Note that W_k^{-1}, N and Π_k are constant matrices. Even if the sector bound a, or equivalently $a_\perp$ varies in time, no time-consuming matrix operations need to be performed on-line because $a_\perp^T W_k^{-1} a_\perp$ is a non-negative scalar.

C. Sector Constraint with Rudder Anti-Chat

In order to remove rudder chattering around zero we propose to translate the sector constraint a distance r^o, more specifically slightly along the x-axis as shown in Figure 6. This modification ensures that the rudder will not be used unless the actuator thrust is above some positive threshold. Furthermore, the transition from zero rudder angle to maximum deflection will be continuous because rudder will be applied gradually as the required thrust along the x-axis increases.

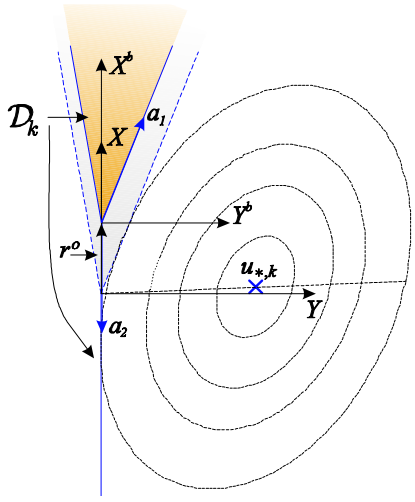

Fig. 6. Translating the sector constraint of thruster k: Defintion of the B-frame.

The distance between the origin of the original O-frame and the origin of the translated B-frame is denoted r^o when it is decomposed in the O-frame. Then, a point c^b in the B-frame is in the O-frame given as $c^o = r^o + c^b$. Thus, the optimal unconstrained solution decomposed in the B-frame is $u_*^b = u_*^o - r^o$.

We may now perform the adjustment due to the sector constraint in the B-frame instead of in the O-frame because $\delta u_k^b = \delta u_k^o$ since the coordinate systems are linearly translated and not rotated with respect to each other. The basic results from the previous section can therefore be applied. More specifically, the cost W_k as given in (26) serves as the weight in the Lagrangian

$$L = \frac{1}{2}\left(\delta u_k^b\right)^T W_k \delta u_k^b + \lambda\left(a_\perp^T u_{*,k}^b + a_\perp^T \delta u_k^b\right) \tag{34}$$

where it must be noted that $a_\perp$ is now given in the B-frame. The minimum cost adjustment is

$$\delta u_k^b = -W_k^{-1} a_\perp \left(a_\perp^T W_k^{-1} a_\perp\right)^{-1} a_\perp^T u_{*,k}^b \tag{35}$$

and the optimal constrained solution u^b and u^o given in the B- and O-frames are

$$u^b = u_*^b + N\left(\Pi_k N\right)^+ \delta u_k^b \tag{36}$$

$$u^o = u_*^o + N\left(\Pi_k N\right)^+ \delta u_k^b \tag{37}$$

A more detailed calculation reveals that

$$\begin{aligned} u^o &= \left(I - NN^T \Pi_k a_\perp \left(a_\perp^T W_k^{-1} a_\perp\right)^{-1} a_\perp^T \Pi_k\right) u_* \\ &\quad + N\left(\Pi_k N\right)^+ W_k^{-1} a_\perp \left(a_\perp^T W_k^{-1} a_\perp\right)^{-1} a_\perp^T r^o \end{aligned} \tag{38}$$

where we notice that the first term is exactly the same as (33), that is when the B-frame coincides with the O-frame, and that the contribution from the translation r^o appears as an additional linear term.

D. The Equicost Line

In case $u_{*,k} \notin \mathcal{D}_k$, we have to decide towards which one of the two nearest boundaries of the feasible domain $\mathcal{D}_k$ we should approach, see Figure 6. Assume that $a_1, a_2 \in \mathbb{R}^2$ are two vectors defining the boundaries of $_k$. We seek the unit vector e_l describing the *equicost line*. That is, for any point on e_l, say $p = ce_l$ where $c \in \mathbb{R}$ is an arbitrary scalar, approaching a_1 and a_2 cost equally much.

Motivated by the results in the two previous sections we know that

$$\delta p_1 = W_k^{-1}(a_1)_\perp \left((a_1)_\perp^T W^{-1}(a_1)_\perp\right)^{-1} (a_1)_\perp^T p \tag{39}$$

$$\delta p_2 = W_k^{-1}(a_2)_\perp \left((a_2)_\perp^T W^{-1}(a_2)_\perp\right)^{-1} (a_2)_\perp^T p \tag{40}$$

are the optimal steps towards a_1 and a_2 respectively. The costs involved are $i = 1..2$,

$$J_i = (\delta p_i)^T W_k \delta p_i = p^T \left((a_i)_\perp \left((a_i)_\perp^T W^{-1}(a_i)_\perp\right)^{-1} (a_i)_\perp^T\right) p \tag{41}$$

and in order to find the equicost line we require $J_1 = J_2$ or $\Delta J = J_1 - J_2 = 0$. Hence,

$$\Delta J = p^T L p = 0 \quad \Leftrightarrow \quad e_l^T L e_l = 0 \tag{42}$$

where $L = L^T$ is given by

$$L = \begin{bmatrix} L_{11} & L_{12} \\ L_{12} & L_{22} \end{bmatrix} = \frac{(a_1)_\perp (a_1)_\perp^T}{(a_1)_\perp^T W_k^{-1} (a_1)_\perp} - \frac{(a_2)_\perp (a_2)_\perp^T}{(a_2)_\perp^T W_k^{-1} (a_2)_\perp} \tag{43}$$

Expanding this expression using $e_l = [x, y]^T$ we obtain the two linear curves where the hyperbola $z = e_l^T L e_l$ intersects the xy-plane, that is

$$L_{11} x^2 + 2L_{12} xy + L_{22} y^2 = 0 \tag{44}$$

Using polar coordinates $e_l = [\cos\theta, \sin\theta]^T$ we get four solutions

$$\theta = \arctan\left(-\frac{L_{12}}{L_{22}} \pm \sqrt{\left(\frac{L_{12}}{L_{22}}\right)^2 - \frac{L_{11}}{L_{22}}}\right) + j\pi \quad j = 0, 1 \tag{45}$$

from which it is straightforward to pick the correct solution, namely the one that lies in the sector spanned by a_1 and a_2. Observe that for this method to be valid, $|L_{22}| > 0$, the infeasible sector has to be less than 180 degrees wide. For propeller/rudder pairs this will always be the case.

E. Restore Continuity

We have already predicted that crossing the equicost line could introduce a discontinuity in u_k^b even if the commanded thrust force τ_c is continuous. In this section a remedy for this situation is proposed, a solution u_k^b that does not necessarily minimize the 2-norm, since that one causes discontinuity. The idea

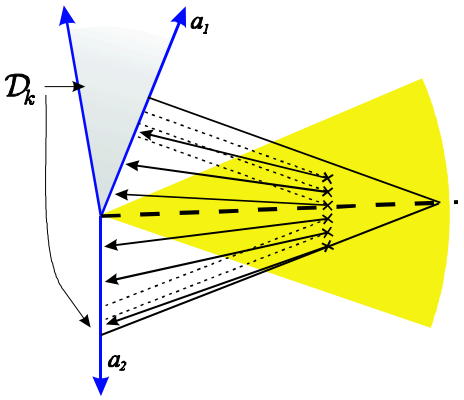

Fig. 7. Translation of $u_{*,k}^b$ without loss of continuity.

is outlined in Figure 7: If $u_{*,k}^b$ is situated inside the sector surrounding the equicost line, we drive u_k^b to a point closer to the origin (the intersection between a_1 and a_2). That is, we follow the solid arrows instead of the dotted lines. Consequently, if $u_{*,k}^b$ lies exactly on the equicost, the desired u_k^b should be zero and continuity will be restored. Figure 8 is a more detailed picture of what we try to accomplish: As we have already calculated the constrained optimal solution u_k^b, marked with a circle, we push it "uphill", in the sense of increased cost, towards the origin.

Decompose $u_{*,k}^b$ onto the unit vectors e_l and e_δ. e_l is parallel to the equicost line and

$$e_\delta = \frac{\delta u_k^b}{\left\|\delta u_k^b\right\|_2} \tag{46}$$

e_l and e_δ define a (not necessarily orthogonal) basis for $\mathbb{R}^2$ such that

$$c = [e_l | e_\delta]^{-1} u_{*,k}^b \tag{47}$$

yields

$$u_{*,k}^b = c_1 e_l + c_2 e_\delta \tag{48}$$

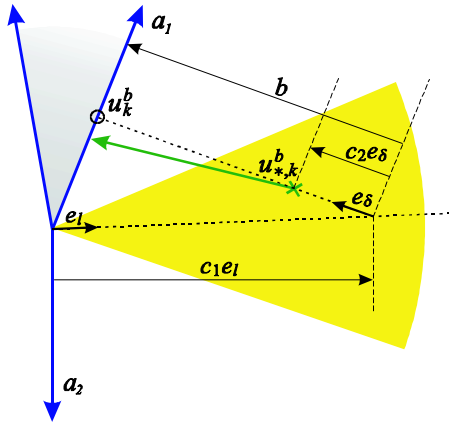

Fig. 8. Detailed picture of restored continuity and definition of basis vectors e_l and e_δ.

The distance between equicost line and $u_{*,k}^b$ is

$$b = u_{*,k}^b + \delta u_k^b - c_1 e_l \tag{49}$$

such that the ratio

$$\gamma = \frac{c_2}{\|b\|_2} \tag{50}$$

says something about where along the line b $u_{*,k}^b$ is located. When γ is close to zero it means that $u_{*,k}^b$ is close to the equicost line, and we would like to force u_k^b toward the origin. The strategy is: Introduce a design parameter $0 < \gamma_r < 1$ and a continuous, non-decreasing weighing function $f : \mathbb{R}_{\geq 0} \to [0, 1]$ and instead of (35), we should use

$$\Delta u_k^b = \left(f\left(\gamma/\gamma_r\right) - 1\right) u_{*,k}^b + f\left(\gamma/\gamma_r\right) \delta u_k^b \tag{51}$$

$$u_k^b = u_{*,k}^b + \Delta u_k^b = f\left(\gamma/\gamma_r\right) \left(u_{*,k}^b + \delta u_k^b\right) \tag{52}$$

It is thus γ_r that determine the width of the sector. Outside the sector, $f\left(\gamma/\gamma_r\right) = 1$ and $\Delta u_k^b = \delta u_k^b$.

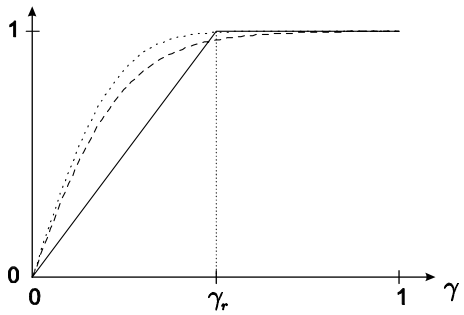

Fig. 9. Weighing functions: $f_1(s) = \text{sat(s)}$ (solid), $f_2(s) = \tanh(2s)$ (dashed) and $f_3(s) = \text{erf}(2s)$ (dotted).

The optimal but discontinuous solution corresponds to $\gamma_r \to 0$ or $f(s) = 1$ for all $s \geq 0$. Figure 9 shows three weighing function alternatives.

F. Proposed Algorithm

The force allocation procedure can be summarized by the following sequence of operations

1. $u_* = A^+ \tau_c$.
2. If $u_* \in \mathcal{D}$ then terminate.
3. Approaching $\mathcal{D}$.
   - Assume thruster k such that $u_{*,k} \notin \mathcal{D}_k$.
   - $u^b_* = u_* - r^o$.
   - Find equicost line e_l and determine towards which boundary a_i of $\mathcal{D}_k$ we should go. Call it a.
   - $\delta u^b_k = -W_k^{-1} a_\perp \left(a_\perp^T W_k^{-1} a_\perp\right)^{-1} a_\perp^T u^b_{*,k}$
4. If $\dim(\mathcal{N}(A)) > 1$
   - Restore continuity of the mapping $\tau_c \rightarrow u^b$
   - $e_\delta = \delta u^b_k / \left\|\delta u^b_k\right\|_2$
   - $c = [e_l | e_\delta]^{-1} u^b_{*,k}$
   - $b = u^b_{*,k} + \delta u^b_k - c_1 e_l$
   - $\gamma = c_2 / \left\|b\right\|_2$
   - $\Delta u^b_k = \left(f\left(\gamma/\gamma_r\right) - 1\right) u^b_{*,k} + f\left(\gamma/\gamma_r\right) \delta u^b_k$
5. If $\dim \mathcal{N}(A) = 1$
   - $\Delta u^b_k = \delta u^b_k$
6. For all thrusters
   - $u^b = u^b_* + N \left(\Pi_k N\right)^+ \Delta u^b_k$
   - $u^o = u^b + r^o$

If the dimension of the null-space of A is less than 2, it is pointless to perform step 4 (Restore continuity) because only a single local minium exists which has to be the global minimizer as well. Likewise, the concept of the equicost line does not apply.

IV. Experiment Description

The experiment was performed in the Guidance, Navigation and Control (GNC) Laboratory at NTNU with the model ship Cybership II (CS2). The boat is a scaled replica of an offshore supply vessel and its overall length is $L_{OA} = 1.255$ meters. It is equipped with three propulsive devices: In the bow there is a small two-bladed RPM-controlled tunnel-thruster capable to produce a sway force, and at the stern there are two RPM-controlled main propellers with rudders.

CS2 is equipped with an onboard PC with a 244 MHz Pentium clone (Cyrix MediaGX) running QNX and is connected to the local LAN through a BreezeCOM 2 Mbit IEEE 802.11 wireless Ethernet link. The control software is developed under Matlab Simulink and Real Time Workshop. Opal RT-Lab handles the compilation of the code as well as any other communication with the target system such as transmission of various signals during the experiments. A graphical user interface (GUI) was developed under LabView

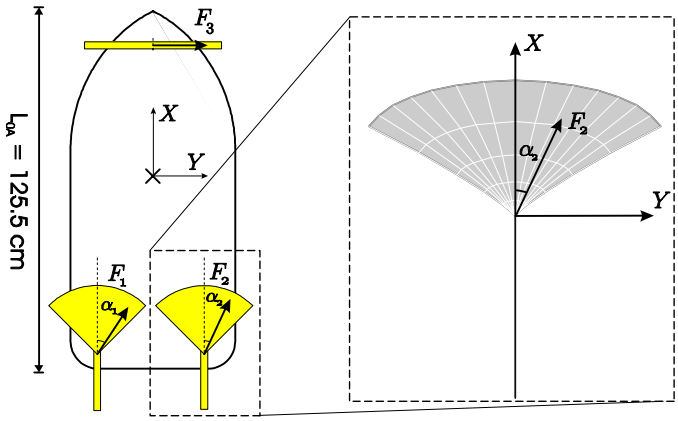

Fig. 10. Outline of Cybership II: Feasible thrust domains.

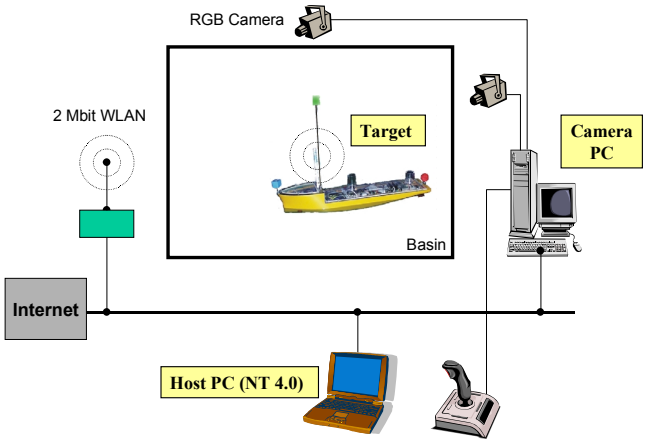

Fig. 11. Overview of the GNC Laboratory

6.0i, together with a manual joystick control system. Through the GUI the operator may switch between different modes of operation while supervising the experiment. The entire system was constructed with standard off-the-shelf hardware and software to keep the costs down.

During start-up CS2 automatically logs on to the camera PC in order to receive position and attitude data. The six DOF positions and orientations (attitude) are measured with two standard RGB cameras with the aid of two MagTrak ISA-cards. This system first locates the three colored markers on CS2 using Tsai's algorithm [20]. An alternative version of the QUEST algorithm [21] based on singular value decomposition instead of eigenvalues calculates the ship's attitude in unit quaternions and converts it to Euler angles, that is the roll, pitch and heading angles. Once the orientation is found, determining the position of the ship is a straightforward operation.

It is reasonable to assume that the rudders are effective when applying positive thrust and we are thus allowed to find general thrust vectors inside the shaded areas in Figure 10.

A. Model Description

At low-speed a surface vessel can be reasonably described by

$$\begin{aligned} \dot{\eta} &= R(\psi)\nu \\ M\dot{\nu} &= -D\nu + \tau + R^T(\psi)b \end{aligned} \tag{53}$$

Here $\eta = [x, y, \psi]^T$ is a vector of position and heading angle. Its components are North position, East position and compass heading, respectively. The body-fixed velocity vector $\nu = [u, v, r]^T$ contains surge, sway and yaw and $\tau \in \mathbb{R}^3$ is the applied thruster force. The matrix $R : \mathbb{R} \to \mathbb{R}^{3\times3}$ describes the rotation between body-fixed and Earth-fixed coordinates:

$$R(\alpha) = \begin{bmatrix} \cos\alpha & -\sin\alpha & 0 \\ \sin\alpha & \cos\alpha & 0 \\ 0 & 0 & 1 \end{bmatrix} \tag{54}$$

and its time derivative can be written $\dot{R} = \frac{d}{dt}(R(\alpha)) = \dot{\alpha}SR(\alpha)$ where S is the skew-symmetric

$$S = \begin{bmatrix} 0 & -1 & 0 \\ 1 & 0 & 0 \\ 0 & 0 & 0 \end{bmatrix} \tag{55}$$

$M \in \mathbb{R}^{3\times3}$ contains the mass of the vehicle, that is the sum of rigid-body and hydrodynamic added mass, and $D \in \mathbb{R}^{3\times3}$ describes linear damping which is assumed to dominate quadratic damping at velocities around zero. Slowly varying disturbances are lumped together in the bias vector $b \in \mathbb{R}^3$. For port-starboard symmetric ships, the surge dynamics can be separated from the sway-yaw part.

A more detailed description of the low-frequency vessel model has been given elsewhere [1].

B. Thruster Model

For fixed pitch propellers the generated thrust force is more or less proportional to the square of the propeller shaft speeds ω_i. The low speed thruster/rudder model for Cybership II can conveniently be separated into two parts. The first one, nominal thrust (rudder angles $\delta_i = 0$, $i = 1, 2$) and the second takes care of rudder lift and drag for positive ω_i.

The nominal thrust is

$$T_i = \begin{cases} k_{iT_p}\omega_i^2 & \omega_i \geq 0 \\ k_{iT_n}|\omega_i|\omega_i & \omega_i \leq 0 \end{cases} \qquad i \in [1..3] \tag{56}$$

Additional rudder forces were found to be

$$L_i = \begin{cases} T_i\left(1 + k_{iLn}\omega_i\right)\left(k_{iL\delta_1}\delta_i + k_{iL\delta_2}|\delta_i|\delta_i\right) & \omega_i \geq 0 \\ 0 & \omega_i \leq 0 \end{cases} \qquad i \in [1, 2] \tag{57}$$

$$D_i = \begin{cases} T_i\left(1 + k_{iDn}\omega_i\right)\left(k_{iD\delta_1}|\delta_i| + k_{iD\delta_2}\delta_i^2\right) & \omega_i \geq 0 \\ 0 & \omega_i \leq 0 \end{cases} \qquad i \in [1, 2] \tag{58}$$

such that for the main propellers, thruster one and two, the surge and sway forces are

$$u_i = \begin{bmatrix} T_i - D_i \\ L_i \end{bmatrix} \tag{59}$$

The thruster and rudder parameters are given in Table I.

Parameter	**Value** $[Ns^2]$
k_{1Tp} , k_{2Tp}	$3.74 \cdot 10^{-3}$
k_{1Tn} , k_{2Tn}	$5.05 \cdot 10^{-3}$
k_{3Tp}	$1.84 \cdot 10^{-4}$
k_{3Tn}	$1.88 \cdot 10^{-4}$

(a) Nominal Thrust Parameters

Parameter	**Value**	**Unit**
k_{1Ln} , k_{2Ln}	$2.10 \cdot 10^{-2}$	s
$k_{1L\delta_1}$, $k_{2L\delta_1}$	0.927	rad^{-1}
$k_{1L\delta_2}$, $k_{2L\delta_2}$	-0.557	rad^{-2}
k_{1Dn} , k_{2Dn}	$9.64 \cdot 10^{-3}$	s
$k_{1D\delta_1}$, $k_{2D\delta_1}$	0.079	rad^{-1}
$k_{1D\delta_2}$, $k_{2D\delta_2}$	0.615	rad^{-2}

(b) Rudder Lift and Drag Parameters

TABLE I

THRUSTER PARAMETERS

C. Control Design

A simple output feedback control law with true integral action is derived to satisfy concept the of the "separation principle" [22] for Euler-Lagrange systems, that is the state estimator and the controller can be independently configured. As long as each component is asymptotically stable, the system as a whole will be so as well.

D. State Feedback Tracking Control

Fossen, Loria and Teel [23] applied adaptive backstepping to obtain integral action, while in Loria, Fossen and Panteley [24] the authors used the bias estimate $\hat{b}$ from the observer. Here we integrate the position error directly (true integral action) and exploit the concept of *commutating matrices* to separate the nonlinear rotations from the otherwise linear dynamics.

Let $\eta_d : \mathbb{R} \to \mathbb{R}^2 \times \mathcal{J}$, $\nu_d : \mathbb{R} \to \mathbb{R}^3$ and $\dot{\nu}_d : \mathbb{R} \to \mathbb{R}^3$ describe desired positions, velocities and accelerations, respectively, such that they together form a smooth reference trajectory. Introduce the deviations $\eta_e = \eta - \eta_d$, $\nu_e = \nu - \nu_d$ and $\dot{\nu}_e = \dot{\nu} - \dot{\nu}_d$. Consider the following tracking control law

$$\begin{aligned} \dot{\xi} &= \eta_e \\ \tau &= -M\left(K_i R^T(\psi)\xi + K_p R^T(\psi)\eta_e + K_d \nu_e\right) + D\nu_d + M\dot{\nu}_d \end{aligned} \tag{60}$$

The last two terms are feed-forward terms. Notice that the gains K_p and K_i are put to the left of $R^T(\psi)$ making them body-fixed gains. This is more intuitive than having them on the right [24], since the compass heading $\psi(t)$ should not influence the convergence rates.

When we use $\dot{\eta}_d = R(\psi)\nu_d$ and define $x = [\xi^T, \eta_e^T, \nu_e^T]^T$ we get the compact form

$$\dot{x} = T^T(\psi) A_c T(\psi) x \tag{61}$$

$$A_c = \begin{bmatrix} 0 & I & 0 \\ 0 & 0 & I \\ -K_i & -K_p & -\left(M^{-1}D + K_d\right) \end{bmatrix} \tag{62}$$

$$T(\psi) = \text{Diag}\left(R^T(\psi), R^T(\psi), I\right) \tag{63}$$

where the Diag()-operator constructs a block-diagonal matrix with zeros on the off-diagonal blocks.

Since the system is controllable, it is possible to assign arbitrary eigenvalues to A_c, and because $T^{-1} = T^T$ for all ψ, the eigenvalues of $T^T(\psi)A_cT(\psi)$ are identical to the ones for A_c. In contrast to linear systems, A_c being Hurwitz is necessary but not sufficient for global exponential stability of (61).

The limiting factor here is the yaw rate $\dot{\psi} = r$. For small r, that is $|r(t)| \leq r_{\max}$, exponential stability of (61) can be shown easily, and if $r_{\max}$ is larger than the physical limit on $|r(t)|$, (61) is stable in a global sense. Increased gains K_i, K_p and K_d results in a larger $r_{\max}$ due to controllability.

Theorem 1: Consider the system (53) controlled by (60). Suppose $|r(t)| \leq r_{\max}$ for all $t \geq t_0$. The origin $x = 0$ of (61) is uniformly locally exponentially stable provided $r_{\max} > 0$ is sufficiently small and if and only if $K_p, K_d, K_i \in \mathbb{R}^{3\times 3}$ are chosen such that A_c as defined by (62) is Hurwitz. If $r_{\max}$ is larger than any physical upper limit for $|r(t)|$, (61) is said to be uniformly globally exponentially stable (UGES).

Proof: Necessity of A_c being Hurwitz is obvious. For proving sufficiency, define $z = T(\psi)x$. By $\dot{T}(\psi)$ we hereby mean $\frac{d}{dt}\left(T(\psi)\right)$. Then,

$$\dot{z} = \dot{T}x + T\dot{x} = \dot{T}T^T z + A_c T x = \left(A_c + rS_T\right) z \tag{64}$$

where $S_T = \text{Diag}(S^T, S^T, 0)$. If and only if A_c is Hurwitz there exists a $P = P^T > 0$ such that for any given $Q = Q^T > 0$

$$PA_c + A_c^T P = -Q \tag{65}$$

Consider the quadratic storage function $V(x) = x^T T^T(\psi) P T(\psi) x = z^T P z$. Its time-derivative

$$\begin{aligned} \dot{V} &= \dot{z}^T P z + z^T P \dot{z} \\ &= z^T \left(A_c^T P + P A_c + r\left(PS_T + S_T^T P\right)\right) z \qquad (66) \\ &\leq -z^T Q z + 2|r_{\max}|\lambda_{\max}(P)\left\|z\right\|_2^2 \\ &= -\left(\lambda_{\min}(Q) - 2|r_{\max}|\lambda_{\max}(P)\right)\left\|x\right\|_2^2 \qquad (67) \end{aligned}$$

is negative definite provided that $r_{\max}$ is small enough. ■

What is the "stability margin", i.e. how large is $r_{\max}$ permitted to be for a given controller before it de-stabilizes the system? From (66) we note that if

$$g(r) = \lambda_{\max}\left(A_c^T P + P A_c + r\left(P S_T + S_T^T P\right)\right) < 0 \tag{68}$$

for all $t \geq t_0$ then (61) is exponentially stable. As $g(r)$ is linear in r it suffices to show $g(-r_{\max}) < 0$ and $g(r_{\max}) < 0$, then $g(r) < 0$ for all $|r(t)| \leq r_{\max}$. We summarize this as follows:

Corollary 2: For a given A_c, a yaw rate bound $r_{\max} > 0$ that guarantees exponential stability of (61) can be found be solving the following generalized eigenvalue problem in the decision variables P and μ

$$\begin{array}{ll} \text{minimize} & \mu \\ \text{subject to} & \left\{ \begin{array}{rcl} P = P^T > 0, \quad \mu > 0 & & \\ P S_T + S_T^T P & < & -\mu\left(A_c^T P + P A_c\right) \\ -P S_T - S_T^T P & < & -\mu\left(A_c^T P + P A_c\right) \end{array} \right. \end{array} \tag{69}$$

where $r_{\max} = 1/\mu$.

This formulation is similar to standard results on stability margins for linear parameter varying (LPV) systems, or polytopic linear differential inclusions [25]. Solving for maximum $r_{\max}$ can be done efficiently using standard software packages [26], but doing that is usually of academic interest only: For well-behaving controllers, the $r_{\max}$ resulting from solving (69) is significantly larger than the highest $|r(t)|$ achievable.

To conclude, low speed tracking control for overactuated ships can be done with linear tools. When the gains have been determined, simply add the proper rotations $R^T(\psi)$ in the control law to make it valid for all heading angles.

E. Observer

A UGES observer estimating low-frequency velocities and positions from position measurements was implemented [27]. More precisely, for the system (53) uniform global exponential convergence of

$$e = \left[\begin{array}{ccc} (\eta - \hat{\eta})^T & (b - \hat{b})^T & (\nu - \hat{\nu})^T \end{array} \right]^T \tag{70}$$

could be expected.

F. Output Feedback Control

Consider the state-feedback controller (60) and substitute the states ν and η with the estimated counterparts $\hat{\nu}$ and $\hat{\eta}$:

$$\begin{array}{rcl} \dot{\xi} & = & \hat{\eta} - \eta_d \\ \hat{\tau} & = & -M\left(K_i R^T(\psi)\xi + K_p R^T(\psi)\left(\hat{\eta} - \eta_d\right) + K_d\left(\hat{\upsilon} - \nu_d\right)\right) + D\nu_d + M\dot{\nu}_d \end{array} \tag{71}$$

Stability of the resulting closed loop system is guaranteed by the following theorem.

Theorem 3: Suppose the tracking error $x = [\xi, \eta_e^T, \nu_e^T]$ of the system (53) subject to the state-feedback controller (60) is UGES and that there exists an observer for which the error e as given by (70) converges uniformly asymptotically to zero. Then, by output-feedback (71) the tracking error x converges uniformly asymptotically to zero.

Proof: Using output-feedback (71) instead of (60), the response (61) is perturbed by the observer errors e. Standard results [28] can be applied if that perturbation term is bounded linearly in e. The proof will then be complete.

By definition $\hat{\eta} = \eta - \tilde{\eta}$ and $\hat{\nu} = \nu - \tilde{\nu}$ which means that $\hat{\eta} - \eta_d = \eta_e - \tilde{\eta}$ and $\hat{\nu} - \hat{\nu}_d = \nu_e - \tilde{\nu}$. Consequently, (71) can be written

$$\begin{aligned} \dot{\xi} &= \eta_e - \tilde{\eta} \\ \hat{\tau} &= -M\left(K_i R^T(\psi)\xi + K_p R^T(\psi)\left(\eta_e - \tilde{\eta}\right) + K_d\left(\nu_e - \tilde{\nu}\right)\right) + D\nu_d + M\dot{\nu}_d \end{aligned} \tag{72}$$

and the vessel dynamics (the x-system) becomes

$$\dot{x} = T^T(\psi)A_c T(\psi)x + T^T(\psi)A_e T_e(\psi)\Pi e \tag{73}$$

Here A_c and $T(\psi)$ are defined in (62)-(63). The parameters in the interconnection term are

$$A_e = \begin{bmatrix} -I & 0 \\ 0 & 0 \\ K_p & \left(M^{-1}D + K_d\right) \end{bmatrix} \tag{74}$$

$$T_e(\psi) = \mathrm{Diag}(R^T(\psi), I) \tag{75}$$

$$\Pi = \begin{bmatrix} I & 0 & 0 \\ 0 & 0 & I \end{bmatrix} \tag{76}$$

Using $z = T(\psi)x$ we get

$$\dot{z} = \left(A_c + \dot{T}T^T\right)z + A_e T_e(\psi)\Pi e \tag{77}$$

and consequently the complete system, the vessel dynamics and observer, can be written on the cascaded form

$$\begin{aligned} \Sigma_1 : \quad \dot{z} &= f_1(t,z) + g(t,z,e) \\ \Sigma_2 : \quad \dot{e} &= f_2(t,e) \end{aligned} \tag{78}$$

where the individual terms of the transformed tracking error system Σ_1 are

$$f_1(t,z) = \left(A_c + \dot{T}T^T\right)z \tag{79}$$

$$g(t,z,e) = A_e T_e(\psi)\Pi e \tag{80}$$

Because $\left\|R^T(\alpha)\right\|_2 = \|R(\alpha)\|_2 = 1$ for all $\alpha \in \mathbb{R}$, $g(t,z,e)$ is indeed linearly bounded in e

$$\|g(t,z,e)\|_2 \leq \|A_e\|_2 \|T_e(\psi)\|_2 \|e\|_2 = \|A_e\|_2 \|e\|_2 \tag{81}$$

■

V. Experimental Results

The main objective of the experiments was to compare the energy consumption with and without active use of rudders during a positioning operation: Move 30 cm sideways while maintaining a fixed heading. This operation is particularly energy consuming when the rudders are not to be used because the ship is unable to produce lateral forces in the stern.

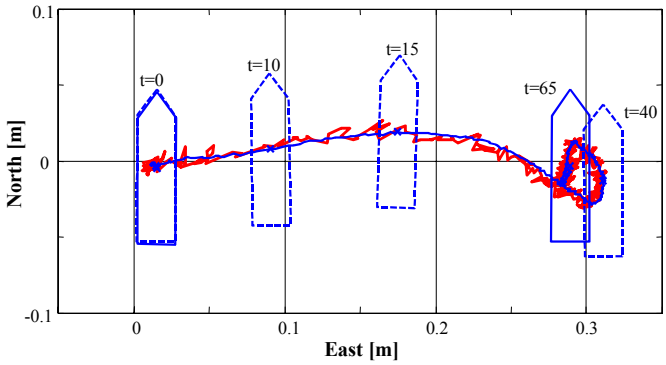

Fig. 12. Operation Overview.

In order to emphasize the differences, at $t = 2$ the desired position changed from $\eta_d = [0, 0, 0]^T$ to $\eta_d = [0, 0.30, 0]^T$ in a step-response fashion, see Figure 12. In full-scale 30 cm corresponds to approximately 20 meters. Measured position is shown in red and the observer's low frequency estimate in blue.

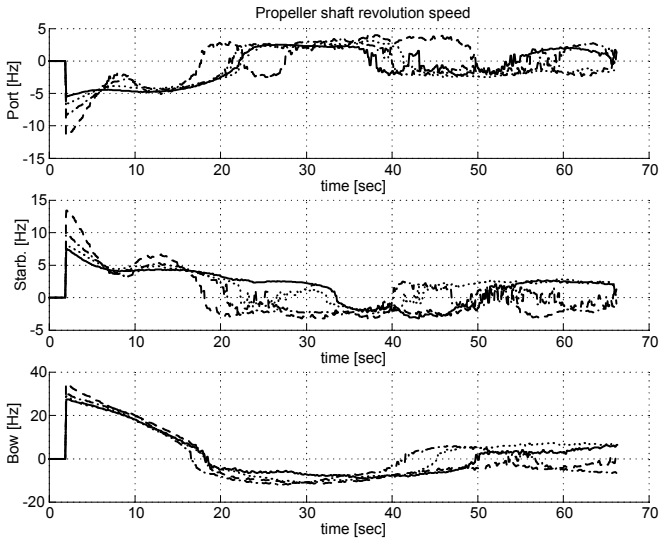

Fig. 13. Propeller shaft speeds ω_i for feasible sector widths $\alpha_{\max} = 0$ (dashed), $\alpha_{\max} = 10$ (dash-dotted), $\alpha_{\max} = 20$ (dotted) and $\alpha_{\max} = 32$ deg (solid).

The rudders were allowed to be deflected inwards. Consequently, the port propeller/rudder pair was allowed to have a lateral component pointing port while the starboard propeller/rudder had a component

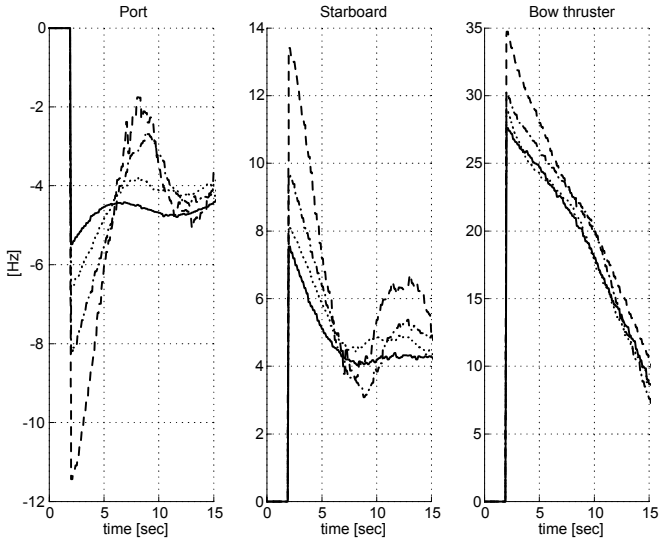

Fig. 14. Propeller shaft speeds ω_i during the first 15 seconds of operation. $\alpha_{\max} = 0$ (dashed), $\alpha_{\max} = 10$ (dash-dotted), $\alpha_{\max} = 20$ (dotted), $\alpha_{\max} = 32$ deg (solid).

pointing in the starboard direction. Two solutions were calculated at each sample. In the first one, u_1, the port rudder was allowed to be used while the starboard rudder was fixed at zero degrees, and in the second one, u_2, the starboard rudder was deflected and the port rudder set at zero degrees. Finally, we picked the solution with minimum 2-norm, that is $\|u_i\|_2$ for $i = 1, 2$.

The feasible sector was varied in four steps from zero to a maximum of 32 degrees, more specifically

$$\alpha_{\max} = \begin{bmatrix} 0 & 10 & 20 & 32 \end{bmatrix}^T \quad \text{deg} \tag{82}$$

In order to attenuate rudder chattering around zero, the following r^o was used for both main propellers

$$r^o = \begin{bmatrix} 1.5 & 0 \end{bmatrix}^T \quad \text{mN} \tag{83}$$

Figure 13 shows the applied propeller revolution speed for all four test runs. The dashed lines are for $\alpha_{\max} = 0$, the dash-dotted lines represent $\alpha_{\max} = 10$, the dotted lines $\alpha_{\max} = 20$ and the solid lines are $\alpha_{\max} = 32$ degrees. Figure 14 is a close-up of Figure 13. The applied rudder angles are plotted in Figure 15. Notice that since the rudders were deflected inwards, the port rudder is always negative while starboard is always positive.

Absorbed hydrodynamic power is proportional to the cube of the shaft speed. We assumed that the efficiency factor was constant so that applied electrical power was proportional to hydrodynamic power. Figure 16 show normalized power, in fractions of the maximum equal to 1, for all four test runs. This way we may compare the individual runs without having an exact power model available. The main propellers' energy consumption defined as the integral of normalized power is reproduced in Figure 17, and the normalized power and energy consumption for the bow thruster is plotted in Figure 18.

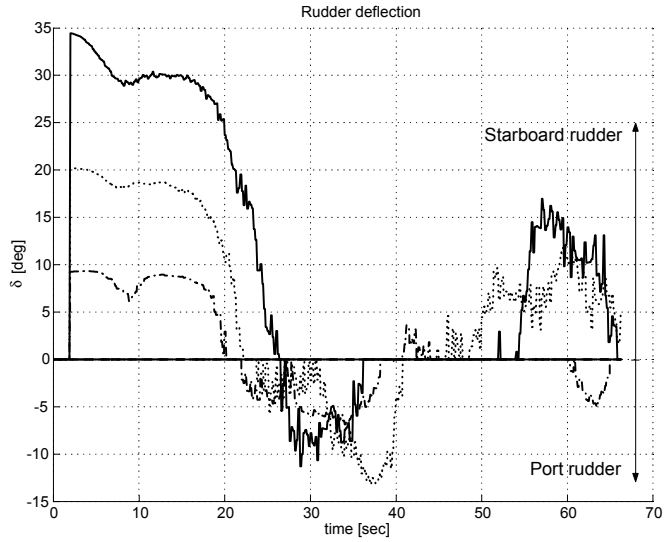

Fig. 15. Rudder angles. $\alpha_{\max} = 0$ (dashed), $\alpha_{\max} = 10$ (dash-dotted), $\alpha_{\max} = 20$ (dotted), $\alpha_{\max} = 32$ deg (solid).

A. Comments

The responses in terms of tracking the desired position were more or less equivalent for all four test runs, and consequently the applied thrust forces τ_c were almost indistinguishable. Time series plots of the positions and thrust forces are not shown.

When the force allocation algorithm is allowed to use the rudders to generate sway forces in the stern, the power and energy consumption for all three propellers decrease significantly. For $\alpha_{\max} = 32$ degrees, the peak in required power for the main propellers is being reduced to only 15% of that required for $\alpha_{\max} = 0$. The peak of the bow thruster's power consumption is reduced by around 50%. When the ship approaches its new position, the differences are less pronounced.

The rudder anti-chattering option, this is a non-zero r^o, works satisfactorily. If this functionality is turned off, the rudder angle set-points would switch between zero and maximum rudder deflection. Measurement noise residues in τ_c spuriously creates an impression of oscillatory rudder behavior (Figure 15).

VI. Concluding Remarks

We have introduced a force allocation algorithm for a sector-restricted thrust device such as a propeller-rudder pair. Handling sector constraints is non-trivial, because the optimization problem is no longer convex and local minima exist. The proposed force allocation method is a three-step algorithm that avoids rudder chattering and ensures a continuous mapping between the commanded thrust force and the extended thrust.

In order to conduct the experiments a semi-global output-feedback tracking control law with integral

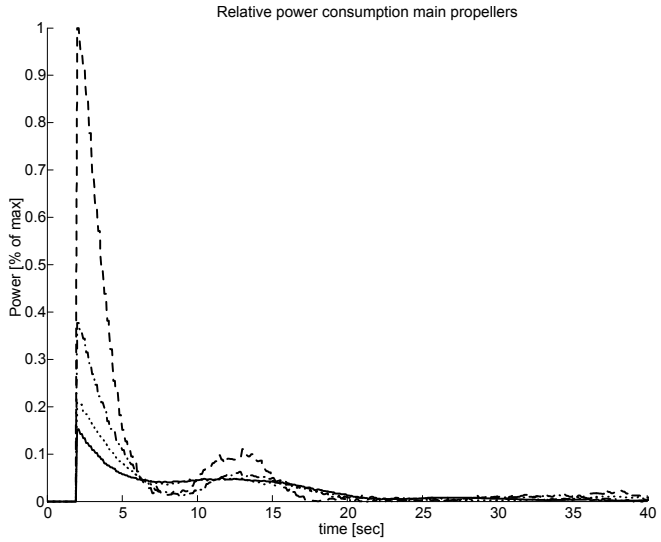

Fig. 16. Normalized power consumption for the main propellers. $\alpha_{\max} = 0$ (dashed), $\alpha_{\max} = 10$ (dash-dotted), $\alpha_{\max} = 20$ (dotted), $\alpha_{\max} = 32$ deg (solid).

action was proposed. Experiments with a model ship confirmed that using rudders actively has a great potential in terms of energy efficiency.

References

[1] T. I. Fossen, *Guidance and Control of Ocean Vehicles*, John Wiley & Sons, 1994.

[2] N. A. Jenssen, *Estimation and Control in Dynamic Positioning of Vessels*, Ph.D. thesis, Dept. of Engineering Cybernetics, Norwegian University of Science and Technology, 1981.

[3] I. Lindfors, "Thrust allocation method for the dynamic positioning system," in *Proc. of the 10th International Ship Control Systems Symposium (SCSS'93)*, Ottawa, Canada, 1993, pp. 3.93–3.106.

[4] O. J. Sørdalen, "Optimal thrust allocation for marine vessels," *Control Engineering Practice*, vol. 5, no. 9, pp. 1223–1231, 1997.

[5] O. J. Sørdalen, "Full Scale Sea Trials with Optimal Thrust Allocation," in *Proc. of the 4th IFAC Conf. on Manoeuvring and Control of Marine Craft (MCMC'97)*, Brijuni, Croatia, 1997, pp. 150–155.

[6] S. P. Berge and T. I. Fossen, "Robust Control Allocation of Overactuated Ships: Experiments With a Model Ship," in *Proc. of the 4th IFAC Conf. on Manoeuvring and Control of Marine Craft*, Brijuni, Croatia, 1997, pp. 166–171.

[7] J. Nocedal and S. J. Wright, *Numerical Optimization*, Springer-Verlag, New York, NY, 1999.

[8] W. C. Durham, "Constrained Control Allocation," *AIAA Journal of Guidance, Control and Dynamics*, vol. 16, no. 4, pp. 717–725, 1993.

[9] W. C. Durham, "Constrained Control Allocation: Three Moment Problem," *AIAA Journal of Guidance, Control and Dynamics*, vol. 17, no. 2, pp. 330–336, 1994.

[10] W. C. Durham, "Attainable Moments for the Constrained Control Allocation Problem," *AIAA Journal of Guidance, Control and Dynamics*, vol. 17, no. 6, pp. 1371–1373, 1994.

[11] K. A. Bordignon and W. C. Durham, "Closed-Form Solutions to Constrained Control Allocation Problem," *AIAA Journal of Guidance, Control and Dynamics*, vol. 18, no. 5, pp. 1000–1007, 1995.

[12] W. C. Durham, "Efficient, Near-Optimal Control Allocation," *AIAA Journal of Guidance, Control and Dynamics*, vol. 22, no. 2, pp. 369–372, 1999.

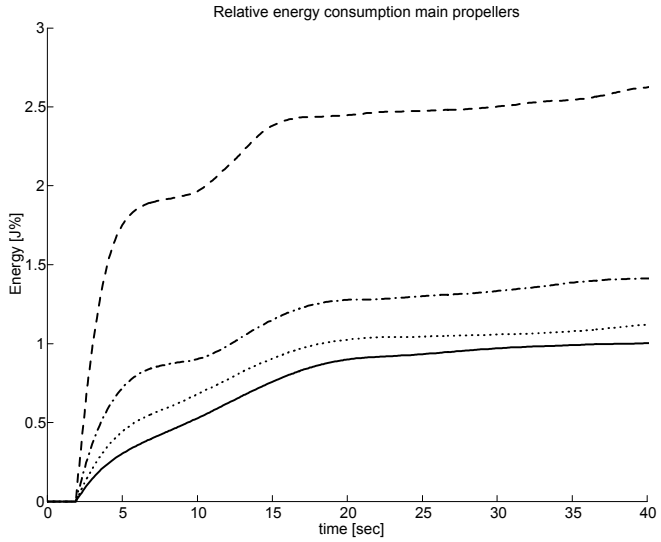

Fig. 17. Consumed energy for the main propellers, given as integrated normalized power. $\alpha_{\max} = 0$ (dashed), $\alpha_{\max} = 10$ (dash-dotted), $\alpha_{\max} = 20$ (dotted), $\alpha_{\max} = 32$ deg (solid).

[13] W. C. Durham, "Computationally efficient control allocation," *AIAA Journal of Guidance, Control and Dynamics*, vol. 24, no. 3, pp. 519–524, 1999.

[14] J. M. Berg, K. D. Hammet, C. A. Schwartz, and S. S. Banda, "An analysis of the destabilizing effect of daisy chained rate-limited actuators," *IEEE Trans. on Control Systems Technology*, vol. 4, no. 2, pp. 171–176, 1996.

[15] J. M. Buffington and D. F. Enns, "Lyapunov stability analysis of daisy chain control allocation," *AIAA Journal of Guidance, Control and Dynamics*, vol. 19, no. 6, pp. 1226–1230, 1996.

[16] J. M. Buffington, D. F. Enns, and A. R. Teel, "Control allocation and zero dynamics," *AIAA Journal of Guidance, Control and Dynamics*, vol. 21, no. 3, pp. 458–464, 1998.

[17] T. A. Johansen, T. I. Fossen, and S. P. Berge, "Constrained nonlinear control allocation with singularity avoidance using sequential quadratic programming," *Submitted to IEEE Trans. on Control Systems Technology*, 2003.

[18] K. A. Bordignon and W. C. Durham, "Null-space augmented solutions to constrained control allocation problems," in *Proc. of the 1995 AIAA Guidance, Navigation and Control Conf. (AIAA-95-3209)*, Baltimore, MD, 1995, vol. 0.

[19] T. A. Johansen, T. I. Fossen, and P. Tøndel, "Efficient optimal constrained control allocation via multi-parametric programming," *Submitted to AIAA J. of Guidance, Control and Dynamics*, 2002.

[20] R. Y. Tsai, "A versatile camera calibration technique for high-accuracy 3D machine vision metrology using off-the-shelf TV cameras and lenses," *IEEE J. of Robotics and Automation*, vol. 3, no. 4, pp. 323–344, 1987.

[21] M. D. Shuster and S. D. Oh, "Three-axis attitude determination from vector observations," *AIAA Journal of Guidance and Control*, vol. 4, no. 1, pp. 70–77, 1981.

[22] A. Loría and E. Panteley, "A separation principle for a class of Euler-Lagrange systems," in *New Directions in Nonlinear Observer Design*, H. Nijmeijer and T. I. Fossen, Eds., pp. 229–247. Springer, 1999.

[23] T. I. Fossen, A. Loria, and A. Teel, "A Theorem for UGAS and ULES of (Passive) Nonautonomous Systems: Robust Control of Mechanical Systems and Ships," *Intl. Journal of Robust and Nonlinear Control*, vol. 11, pp. 95–108, 2001.

[24] A. Loría, T. I. Fossen, and E. Panteley, "A separation principle for dynamic positioning of ships: Theoretical and experimental results," *IEEE Trans. on Control Systems Technology*, vol. 8, no. 2, pp. 332–343, 2000.

[25] S. Boyd, L. El Ghaoui, E. Feron, and V. Balakrishnan, *Linear Matrix Inequalities in System and Control Theory*, Society for Industrial and Applied Mathematics SIAM, Philadelphia, PA, 1994.

[26] P. Gahinet, A. Nemirovski, A. J. Laub, and M. Chilali, *LMI Control Toolbox*, The Mathworks Inc., 1995.

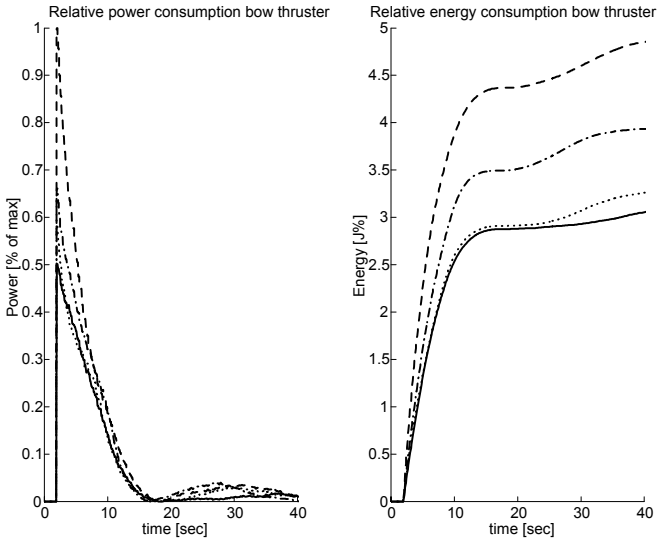

Fig. 18. Normalized power and energy consumption of the bow thruster. $\alpha_{\max} = 0$ (dashed), $\alpha_{\max} = 10$ (dash-dotted), $\alpha_{\max} = 20$ (dotted), $\alpha_{\max} = 32$ deg (solid).

[27] K.-P. Lindegaard and T. I. Fossen, "A model based wave filter for surface vessels using position, velocity and partial acceleration feedback," in *Proc. of the 40th IEEE Conf. on Decision and Control*, Orlando, FL, 2001.

[28] E. Panteley and A. Loria, "On global uniform asymptotic stability of nonlinear time-varying non-autonomous systems in cascade," *Systems & Control Letters*, vol. 33, no. 2, pp. 131–138, 1998.